Research Article

Terahertz-Induced Second-Harmonic Generation in Quantum Paraelectrics: Hot-Phonon Effect

Fei Yang[1], X. J. Li[1], Diyar Talbayev[2], Long-Qing Chen[1]

1. Department of Materials Science and Engineering and Materials Research Institute, Pennsylvania State University, United States; 2. Department of Physics and Engineering Physics, Tulane University, United States

Recent terahertz-pump second-harmonic-generation(SHG)-probe measurements of quantum paraelectrics observed a significant long-lived non-oscillatory SHG component following an ultrafast resonant excitation of the soft mode, which was interpreted as a signature of terahertz-induced transient ferroelectric order. Here we propose a temperature-dependent dynamic model incorporating the hot-phonon effect to simulate the soft-mode behaviors under ultrafast terahertz excitation. Its application to paraelectric $KTaO_3$ produces quantitatively most of the features exhibited in our time-resolved SHG measurements and those in existing literature, including a long-lived non-oscillatory SHG response, SHG oscillations at twice the soft-mode frequency, SHG dampings as well as temperature and field-strength dependencies. We conclude that the observed terahertz-induced non-oscillatory SHG response in quantum paraelectrics is a consequence of the induced nonequilibrium hot-phonon effect, offering an alternative to its existing interpretation as a signature of transient ferroelectric order.

Corresponding authors: D. Talbayev, dtalbayev@gmail.com; L. Q. Chen, lqc3@psu.edu

Introduction

The quantum criticality in condensed matter physics describes the ordering of a quantum phase that occurs at/near zero temperature. This phenomenon has attracted considerable attention, partly due to its distinct characteristics and unexpected physics arising from the low-lying collective excitations. Extensive research over the past few decades has suggested the presence of the quantum criticality in certain strongly-correlated materials, but which are often complex with various intertwined quantum

 doi.org/10.32388/8Y19C2

orders. A notable exception is the displacive quantum paraelectrics[1][2][3][4][5][6], where there is a strong competition between quantum fluctuations and ferroelectric ordering. This class of material is supposed to transition from the paraelectric to ferroelectric states at low temperature due to the lattice dynamical instability[5][7][1][8][3], but the zero-point lattice vibrations prohibits the long-range ferroelectric order[1][5][6][7], leading to an incipient ferroelectricity, sometimes referred to as hidden ferroelectric phase[9][10].

While doping[11][12][13][14] or isotope substitution[15][2] can turn quantum paraelectrics to ferroelectrics, transiently reaching the hidden ferroelectric phase through ultrafast manipulation with intense femtosecond-pulsed laser[16][17][18][19] is particularly appealing, given its promising potential for applications in memory and computational devices[20][21]. One strategy is to coherently drive the so-called soft-phonon mode—associated with the lattice dynamical instability[22][23][24][25]—into the nonlinear regime, aiming to create transient ferroelectric order. For this purpose, several terahertz(THz)-pumped second-harmonic-generation(SHG)-probe measurements have been performed in the protypical displacive quantum paraelectrics, $SrTiO_3$[9] and $KTaO_3$ single crystals[10][26]. At low temperatures, a significant long-lived non-oscillatory SHG component, superimposed by a clear SHG oscillation at twice the soft-mode frequency, was observed after a THz pulse[9][10][26]. The origin and precise mechanisms of this non-oscillatory component and soft-mode frequency doubling phenomenon[9][10][26] remain unclear[27][28]. The observed non-oscillatory SHG background is commonly interpreted as a signature of a THz-induced transient ferroelectric order, possibly arising from a THz-driven intrinsic lattice displacement[9], or from a THz-induced long-range correlation between extrinsic local polar structures by defects[10]. However, such an interpretation seems to contradict several other findings. For example, it was realized that the THz pulses up to 500 kV/cm were insufficient to produce a global intrinsic ferroelectricity[10], whereas inducing a long-range correlation between extrinsic defect dipoles via an ultrafast manipulation does not require coherently driving an intrinsic soft mode. More importantly, soft modes are experimentally observed to go through hardening with an increasing THz-field strength[9][10][26], suggesting an intense THz field drives the quantum paraelectrics away from rather than towards ferroelectricity, since the soft-mode hardening in displacive paraelectrics is an indicator of departure from ferroelectricity.

On the other hand, similar non-oscillatory components in pump-probe measurements have been commonly observed in other subfields, e.g., in measurements of the interband transitions in

semiconductors (e.g., graphene[29]) and collective excitations in superconductors[30][31][32][33][34], and they were attributed to the induced nonequilibrium hot-quasiparticle effect. For example, in superconductors, by using intense THz pulses, one can resonantly excite the amplitude mode of the superconducting order parameter[30][31][32][35][36], namely the Higgs-mode excitation[37]. In most of the measurements, a non-oscillatory component was observed and can persist for a long time after the THz pulse[30][31][32], as a consequence of the nonequilibrium hot-quasiparticle effect[30][31][32][33][34]. In contrast, such a hot-quasiparticle effect in ultrafast-optical responses of ferroelectrics and paraelectrics has largely been overlooked.

In this work, we propose a temperature-dependent dynamic model to describe the soft-mode behaviors under an ultrafast resonant excitation by incorporating the hot-phonon effect, and examine the THz-induced SHG responses in displacive quantum paraelectric $KTaO_3$ using a combination of theoretical and experimental studies. Numerical simulations based on the developed dynamic model quantitatively produce all the main features exhibited in our time-resolved SHG measurements, including a long-lived non-oscillatory SHG response, SHG oscillations at twice the soft-mode frequency, SHG dampings as well as temperature and field-strength dependence. We therefore attribute the THz-induced non-oscillatory SHG component to the nonequilibrium hot-phonon effect, offering an alternative to its existing interpretation as a signature of transient ferroelectric order in quantum paraelectrics[9][10][26].

Furthermore, we also explore the SHG responses of a ferroelectric $KTaO_3$ after an ultrafast THz excitation to understand the individual responses of actual ferroelectric nano-regions (e.g., extrinsic local polar structures by defects in quantum paraelectrics[10]). In this case, both our theoretical simulations and experimental measurements show a THz-induced long-lived SHG oscillation at the single polar-mode frequency without any evident signature for the non-oscillatory component, in contrast to the observed SHG response of quantum paraelectrics under an ultrafast THz excitation, suggesting that the previously reported resonant SHG features in quantum paraelectrics does not come from ferroelectric nano-regions.

Experimental setup.—We use intense single-cycle THz pump pulses (up to 210kV/cm), generated from the optical rectification in a $LiNbO_3$ prism[26], to resonantly excite the soft mode in a quantum paraelectric $KTaO_3$ single crystal and detect the time-resolved SHG signal via a femtosecond optical-frequency (800-nm) probe pulse as a function of delay time with respect to the pump pulse. The field

directions of the THz pump and the optical-frequency probe pulses are both set along the [100] direction in $KTaO_3$ crystal. The time-resolved signal is measured using a GaP photodiode and a blue filter after the $KTaO_3$ sample, which eliminates the fundamental 800-nm wavelength from the detected light. The waveform of the employed single-cycle THz pump pulses is shown in Fig. 1(b). More details can be found in Supplemental Materials.

Dynamic model.—Optical excitation of the soft mode in quantum paraelectrics is known to induce an electrical polarization $\mathbf{P} = u_{\mathrm{sp}}(\sum_i Q_i \mathbf{e}_i)/\Omega_{\mathrm{cell}}$[38][39][40][3][41][42][43][44], with u_{sp} being the soft-mode displacement; Q_i and $\mathbf{e}_i$ standing for the charges and eigenvectors of the related ions (in a unit cell of volume Ω_{cell}) in the soft mode, respectively. As a result of lattice dynamics, its effective Lagrangian can be written as

$$\mathcal{L}_{\mathrm{eff}} = \frac{m_p}{2}(\partial_t P)^2 - \left[\frac{\alpha(T)}{2}P^2 + \frac{b}{4}P^4 - \mathbf{E}(t)\cdot\mathbf{P}\right], \tag{1}$$

where b is an anharmonic coefficient, related to three-soft-phonon interactions; m_p denotes the effective mass[38]; $\mathbf{E}(t)$ represents the THz field; $\alpha(T)$ is the harmonic coefficient, and using the self-consistent renormalization theory within the path-integral approach[6], the equilibrium harmonic coefficient is derived as $\alpha_e(T) = \alpha_e(T=0) + bC(T)$ (see Supplementary Materials). Here, $C(T)$ requires a self-consistent formulation of the bosonic thermal excitation of the soft phonons:

$$C(T) = \frac{\hbar}{m_p}\sum_{\mathbf{q}}\left[\frac{2n_q^{(0)}+1}{\omega_q(T)} - \frac{1}{\omega_q(T=0)}\right], \tag{2}$$

where $n_q^{(0)} = 1/\{\exp[\hbar\omega_q/(k_B T)] - 1\}$ is the equilibrium distribution function (Bose distribution) of the soft phonons, and the energy spectrum of the soft phonons is given by

$$\omega_q(T) = \sqrt{[\alpha_e(T=0) + bC(T)]/m_p + v^2 q^2}, \tag{3}$$

with v being the mode velocity. Mathematically, $C(T)$ in Eq. (2) increases monotonically with temperature, and as seen from Eq. (3), this monotonic increase describes the soft-mode hardening [i.e., the increase of soft-phonon excitation gap $\omega_{q=0}(T)$] with temperature, consistent with the known behavior of the soft modes in quantum paraelectrics[22][23][24][25].

The ultrafast THz field $\mathbf{E}(t)$ can stimulate the dynamics of $\mathbf{P}(t) = \mathbf{P}_0 + \delta\mathbf{P}(t)$, and in particular, a nonequilibrium distribution $n_q = n_q^{(0)} + \delta n_q(t)$ of the soft phonons, thereby leading to the evolution of $\alpha(t) = \alpha_e + \delta\alpha(t)$ according to Eq. (2). Using the Euler-Lagrange equation[45], one can find the equation of motion for the polarization:

$$m_p \partial_t^2 \mathbf{P} + \gamma \partial_t \mathbf{P} = -\alpha(t)\mathbf{P} - bP^2\mathbf{P} + \mathbf{E}(t). \quad (4)$$

Here, we have introduced a damping term, with γ being the damping rate. This damping should be dominated by three-phonon scattering between two soft phonons and one acoustic phonon, leading to a T-dependent $\gamma(T)$. In principle, the evolution of $\alpha(t)$ should incorporate a fully microscopic bosonic Boltzmann equation of the soft phonons. However, such a microscopic treatment is complex and will not change the main results and conclusions in this work. Thus, here we employ the Allen-Cahn-like relaxation equation extensively used in the phase-field method[46] (see Supplemental Materials):

$$\partial_t \delta\alpha(t) = -\eta(P^2 - P_0^2)/2 - \delta\alpha/\tau_E, \quad (5)$$

where we take $\eta < 0$ since the soft-phonon number increases after the excitation and leads to the increase of $\alpha(t)$ according to Eq. (2); τ_E is the energy-relaxation time of the system.

For quantum paraelectrics, we first self-consistently solve the coupled Eqs. (2) and (3) using only the knowledge about the ground-state parameters $\alpha_e(T = 0)$ and b, to obtain the equilibrium $\alpha_e(T) > 0$, and hence, $P_0^2 \equiv 0$. We then solve the dynamic equations [Eqs. (4) and (5)] using the experimental waveform of the single-cycle THz pump pulse [Fig. 1(b)] as the input field $\mathbf{E}(t)$, resulting in the temperature-dependent dynamics of the soft mode under an ultrafast excitation.

It has been established that the inverse dielectric function $1/\varepsilon(T) \propto \alpha(T)$ in quantum paraelectrics[2] [6], thereby leading to the THz-induced SHG intensity $\delta \mathrm{I}_{\mathrm{SHG}}(t) \propto \delta\alpha(t)$ (See Supplemental Materials). In specific simulations, we consider the damping rate $\gamma(T)$ as the only fitting parameter for temperature variation in the experimental measurements. Other parameters used in simulations are based on several independent experimental measurements (See Supplementary Materials).

Results.—Figures 1(d) and 1(e) show the theoretically predicted and experimentally measured time-resolved SHG responses under THz excitation at different temperatures, respectively. At a low temperature of 20 K, the THz field can coherently drive the soft-mode into a strong nonlinear resonant state, showing clear oscillations on top of a non-oscillatory background after the THz stimulation ($t > 2$ ps). These resonant features can persist up to 8 ps at 20 K, and gradually ebb away as temperature increases. At a high temperature of 200 K, the SHG response becomes weak and only follows the square of the THz waveform [Fig. 1(b)], because the soft mode moves out of the range of the THz spectrum due to its hardening with increase in temperature. All of these THz-induced SHG

features are consistent with the previously reported findings in quantum paraelectrics $SrTiO_3$[9] and $KTaO_3$[10][26].

For a direct comparison, we plot the theoretical and experimental results together in Fig. 2(a), which demonstrates a remarkably quantitative agreement between our theoretical predictions and experimental measurements in all aspects of the THz-induced SHG responses of the quantum paraelectric. It should be emphasized that after the zero-temperature parameters are determined from independent measurements, our simulation achieves this good agreement in both temperature variation and temporal evolution by fitting only a single parameter, the temperature-dependent damping rate $\gamma(T)$.

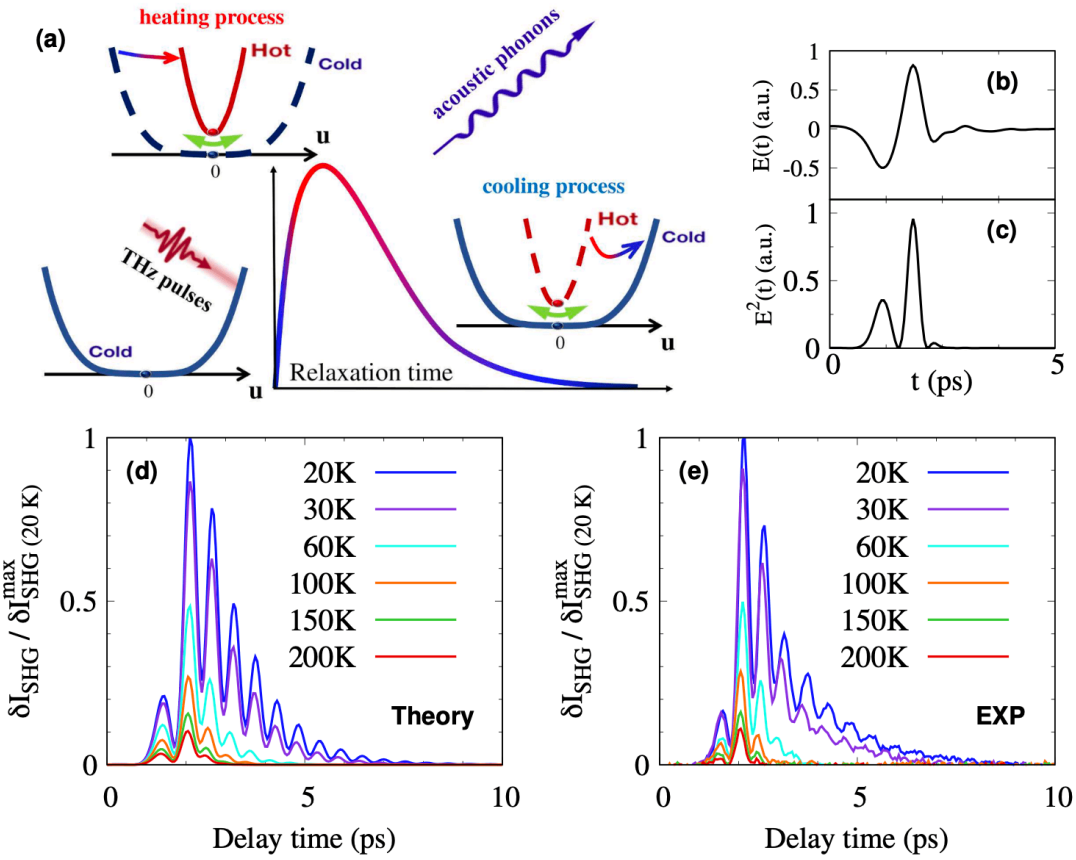

Figure 1. (a) Schematic illustration of the generation (heating process) and decay (cooling process) of the hot-phonon effect during a nonlinear ultrafast resonant excitation, which creates a long-lived non-oscillatory SHG component. (b) The waveform and (c) waveform squared of the single-cycle THz pump pulse employed in experiments and simulations. (d) Theoretically calculated and (e) experimentally measured time-resolved SHG in paraelectric $KTaO_3$ at different T.

To gain more insight into these emerging SHG characters of quantum paraelectrics under a THz excitation, we carefully examine the temperature-dependent behaviors of the soft-mode hardening and the SHG damping. Figure 2(b) shows the FFT of the measured SHG oscillatory component, which was acquired by subtracting the non-oscillatory SHG component from the original signal. At 20 K, a single mode emerges around 1.8 THz, and it gradually hardens as temperature increases. This is consistent with the established soft-mode behavior of $KTaO_3$ reported in previous studies[10][26]. It should be emphasized that the soft mode in quantum paraelectric $KTaO_3$ is reported to downshift to 0.8-0.9 THz below 50 K[22][23][24][25]. Thus, the THz-induced SHG oscillations in both our theory and

doi.org/10.32388/8Y19C2

experiment oscillate at twice the soft-mode frequency. This soft-mode frequency doubling phenomenon[9][10][26] is expected in quantum paraelectrics lying at the verge of the central-symmetric state, which we will discuss its origin later. The extracted soft-mode frequencies from experiments and the simulations [$\omega_{q=0} = \sqrt{\alpha_e(T)/m_p}$] are plotted together in Fig. 2(c) as a function of temperature and they exhibit an excellent quantitative agreement in their temperature dependence.

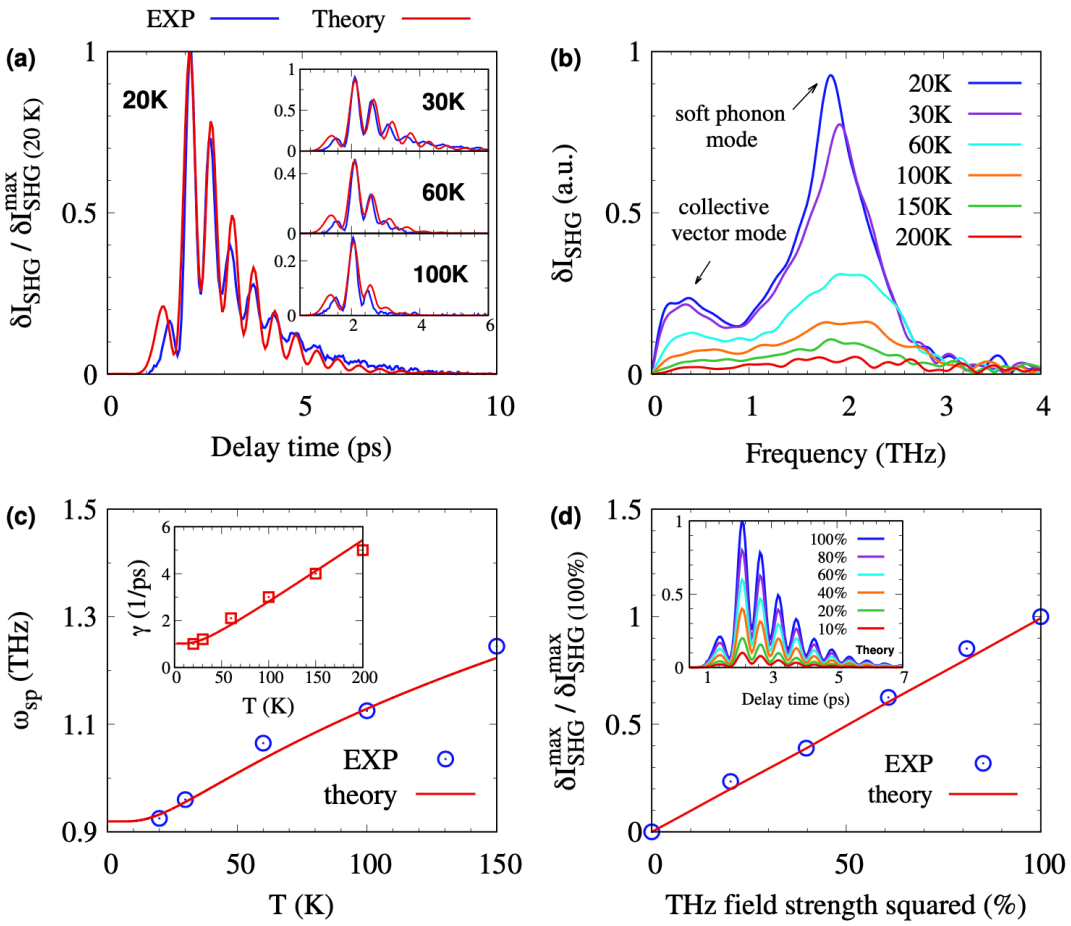

Figure 2. (a) Detailed comparison between theoretical and experimental results of the time-resolved SHG signal. (b) Fourier transform of the measured SHG oscillations at different temperatures. It is noted that at temperatures below 100 K, besides the widely reported soft mode that emerges around 1.8 THz, there exists another mode around lower frequency of 0.4 THz, which should correspond to a collective vector mode emerged in displacive ferroelectrics and quantum paraelectrics as proposed in Ref.[6]. (c) Theoretical and experimental results of the soft-mode excitation gap. The inset shows the employed damping rate $\gamma(T)$ (squares) in our simulation, and a fitting curve: $\gamma(T) \propto 1 + 2/[\exp(T_{ac}/T) - 1]$ with $T_{ac} = 76$K. (d) SHG peaks as a function of THz-field power at 20 K. The inset shows the numerical time-resolved SHG signal at different field strengths.

For an analytical analysis of the THz excitation, we assume a pump field in the single-frequency form: $\mathbf{E}(t) \approx \mathbf{E}_0 \cos(\Omega t)$, with Ω being the THz-field frequency. From Eqs. (4) and (5), neglecting all

doi.org/10.32388/8Y19C2

damping terms, one approximately has $\partial_t \delta\alpha(t) \approx \frac{|\eta| E_0^2 \cos^2(\Omega t)}{2[m_p(\omega_{q=0}^2 - \Omega^2)]^2}$ (see Supplementary Materials), leading to the THz-induced dynamic behavior of $\delta\alpha(t)$:

$$\delta\alpha(t) \approx \frac{|\eta| E_0^2 \sin(2\Omega t)/(2\Omega)}{m_p^2[(2\omega_{q=0})^2 - (2\Omega)^2]^2} + \frac{|\eta| E_0^2 t}{m_p^2[(2\omega_{q=0})^2 - (2\Omega)^2]^2}. \quad (6)$$

The first term in the right-hand side of the above equation contributes to the SHG oscillations, induced by the second order of the THz pump field. This second-order response to a THz field leads to the aforementioned soft-mode frequency doubling phenomenon, since for an ultrafast (δ-function) pulse, it becomes $|\eta| E_0^2 \sin(2\omega_{q=0} t)/(8 m_p^2 \omega_{q=0}^2)$ in the response theory of a resonant excitation. The second term leads to the generation of a non-oscillatory SHG component, and it describes the nonequilibrium hot-phonon effect under the nonlinear excitation because it pushes the total $\alpha(t)$ towards a higher positive value, proportional to the power $E_0^2 \sigma$ of the THz pulse, with σ being the THz-pulse temporal width. In addition, by Eq. (6), one can also infer that a significant non-oscillatory SHG component and large SHG oscillations are possible only at the resonant-excitation condition of $\omega_{q=0}(T) = \Omega$, in agreement with our numerical simulations and experimental observations in the temperature-dependent SHG signal [Fig. 1(d) and 1(e)].

Our numerical and experimental results for the SHG signal peaks as a function of the THz-field power are plotted in Fig. 2(d). Clearly, they are proportional to the THz-field power, i.e., $\delta \mathrm{I}_{\mathrm{SHG}} \propto E_{\mathrm{pump}}^2 E_{\mathrm{probe}}^4$, as also observed in the previous measurements[9][10][26] and in agreement with the analysis above in Eq. (6). This suggests that the THz-induced SHG response in quantum paraelectrics is a second-order response to the THz pump field, a near-equilibrium response, rather than the intricate far-from-equilibrium dynamics that usually manifests at higher-order responses, and there is no generation of a transient ferroelectric order. Actually, it should be emphasized that a finite SHG signal detected by the 800-nm probe field with frequency of 1.55 eV in fact can not justify the emergence of ferroelectric order (see Supplementary Materials).

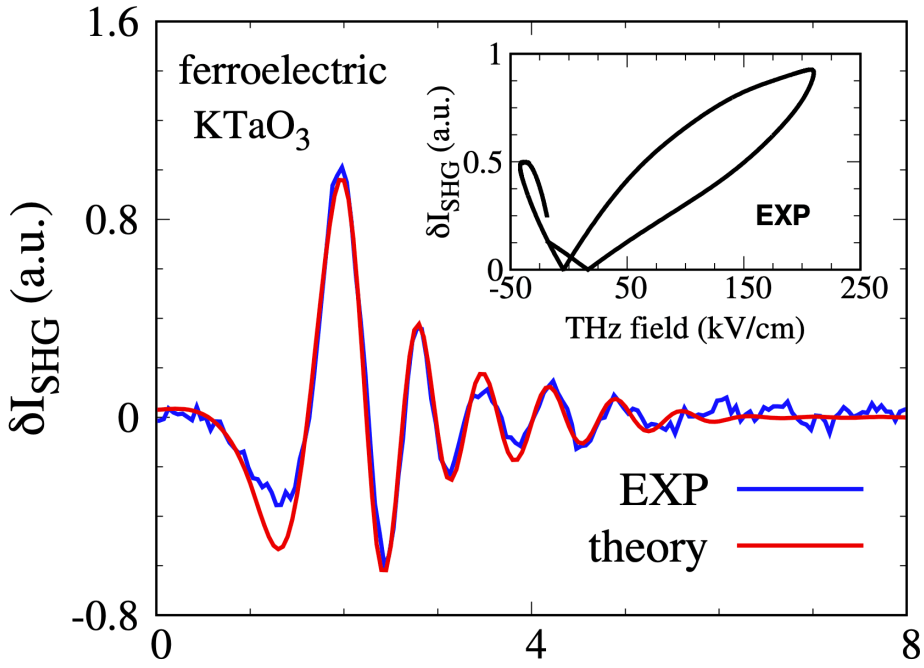

Figure 3. Numerical simulation and experimental measurement of the time-resolved SHG signal in ferroelectric $KTaO_3$ at 77 K. The inset shows the measured hysteresis loop of this sample at 77 K.

For the damping, there are two distinct relaxation processes going on after an ultrafast excitation: soft-mode damping $\gamma(T)$ and energy relaxation $1/\tau_E$. We find that the soft-mode damping dominates the damping of the THz-induced resonant SHG features as it should be, and it can be well described by the three-phonon (two soft phonons and one acoustic phonon) scattering mentioned above. Specifically, according to the microscopic scattering mechanism for calculating the scattering probabilities of the acoustic-phonon emission and absorption[47][48], the damping rate of the soft mode can be approximated as $\gamma(T) \propto 2\overline{n}_{ac}(T) + 1 \approx \frac{2}{e^{T_{ac}/T}-1} + 1$, with $\overline{n}_{ac}(T)$ being the averaged acoustic-phonon number and T_{ac} being a characteristic temperature. Then, the temperature dependence of $\gamma(T)$, obtained by fitting to our time-resolved experiments, can be well captured, as illustrated in the inset of Fig. 2(c).

Finally, it is noted that to explain the observed long-lived non-oscillatory SHG component, Cheng et al. has proposed a potential origin in Ref.[10], a THz-induced correlation between the local polar structures (i.e., ferroelectric nano-regions) that arise from the extrinsic defects, leading to a global

ferroelectric-like response. To examine this possibility, we explore the THz-induced SHG response of a ferroelectric $KTaO_3$, experimentally obtained through an annealing process under high vacuum[1]. We then conducted the THz-pump SHG-probe measurements on the ferroelectric $KTaO_3$ crystal, and the results are plotted in Fig. 3. As shown in Fig. 3, the ferroelectric $KTaO_3$ exhibits a totally different THz-induced SHG responses from the quantum paraelectric $KTaO_3$. The THz-field strength dependence of the SHG response (inset of Fig. 3) shows a clear butterfly-shape hysteresis loop, which demonstrates the presence of the ferroelectricity. As for the time-resolved SHG signal (Fig. 3), a clear oscillation develops after the THz pulse ($t > 2$ps) and persists up to 7 ps, suggesting a coherent/resonant driving of a collective excitation (i.e., a polar mode). However, no evident non-oscillatory component was observed, and no polar-mode frequency doubling phenomenon occurs in the resonant excitation as the observed SHG response during the pump pulse ($t < 2$ ps) just follows the pump-pulse waveform [Fig. 1(b)]. This suggests that the THz-induced SHG signal in ferroelectric $KTaO_3$ is a linear response to the THz pump field, i.e., $\delta \mathrm{I}_{\mathrm{SHG}} \propto E_{\mathrm{pump}} E_{\mathrm{probe}}^4$ as a consequence of the breaking of the global lattice inversion symmetry by the existing ferroelectric order. These resonant features in the ferroelectric state are in contrast to the ones in the quantum paraelectric state, and therefore, it should suggest that the ferroelectric nano-regions are not the origin for the observed SHG resonant features in the quantum paraelectrics.

For numerical simulations of the ferroelectric state, we set a negative value for α_e at $T = 77$K to fit our experimental measurement of ferroelectric $KTaO_3$, and it leads to a finite equilibrium $P_0^2 = -\alpha_e/b$. Then, we perform the simulation on the basis of the dynamic model, and as shown in Fig. 3, the produced results can well capture the experimental measurements. Following the derivation of Eq. (6), the THz-induced dynamic behavior of $\delta\alpha(t)$ in the ferroelectric $KTaO_3$ reads

$$\delta\alpha \approx |\eta| \frac{(\mathbf{P}_0 \cdot \mathbf{E}_0)\sin(\Omega t)}{m_p \Omega(\Delta^2 - \Omega^2)} + |\eta| E_0^2 \left[\frac{\sin(2\Omega t)}{(2\Omega)} + t\right] \frac{1}{4\Omega[m_p(\Delta^2 - \Omega^2)]^2}, \tag{7}$$

with $\Delta = \sqrt{-2\alpha_e/m_p}$ being the polar-mode excitation gap. Consequently, the presence of the ferroelectric order leads to the emergence of a linear response (first term) to the THz field, in agreement with our numerical simulations and experimental measurements as well as symmetry analysis. This response dominates the THz-induced SHG signal at a relatively weak THz field, whereas the hot-phonon effect (non-oscillatory component) and soft-mode frequency doubling phenomenon that manifest in second-order excitation, i.e., second term, are masked in the THz-induced SHG response.

In summary, by combining numerical simulations based on a developed dynamic model and experimental measurements on the THz-induced time-resolved SHG responses in paraelectric $KTaO_3$, we conclude that the observed long-lived non-oscillatory component under an ultrafast excitation in recent THz-pump SHG-probe experiments[9][10] is a consequence of the induced nonequilibrium hot-phonon effect. Actually, based on this understanding of the hot-phonon effect, the previously observed soft-mode hardening as THz-field strength increases[9][10][26] can also be understood: the increase in the field strength enhances the hot-phonon effect and promotes the soft-phonon temperature during the nonequilibrium process, thereby leading to a soft-mode hardening.

Acknowledgements

F.Y. and X.J.L. did the theoretical and experimental studies, respectively, and contributed equally to this work. F.Y. and L.Q.C. acknowledge support from the US Department of Energy, Office of Science, Basic Energy Sciences, under Award Number DE-SC0020145 as part of Computational Materials Sciences Program. F.Y. and L.Q.C. also appreciate the generous support from the Donald W. Hamer Foundation through a Hamer Professorship at Penn State. X.J.L. and D.T. acknowledge support by the National Science Foundation under Grant No. DMR-1554866.

Footnotes

[1] After the annealing under high vacuum, we observe that KTaO3 transitions to a ferroelectric state. The exact mechanism driving this transition remains unclear and is currently under our in- vestigation. One plausible explanation is the potential influence of the Sn or Fe doping introduced from environment during annealing, similar to the transitions to a ferroelectric state ob- served in Fe-doped KTaO3[49] and Nb-doped KTaO3[50][51]. Notably, the origin of this equilibrium transition does not affect the conclusions of the present nonequilibrium study on ultra- fast optical responses, as similar phenomena have been widely observed in pump-probe measurements of other ferroelectric materials[52][53][54].

References

1. a, b, c *Müller KA, Burkard H (1979). "Phys. Rev. B." **19**: 3593.*

2. ^a ^b ^cRowley S, Spalek L, Smith R, Dean M, Itoh M, Scott J, Lonzarich G, Saxena S (2014). "". Nat. Phys.. **10**: 367.
3. ^a ^b ^cCowley RA (1996). "Philos. Transact. A Math. Phys. Eng. Sci.". **354**: 2799.
4. ^Fujishita H, Kitazawa S, Saito M, Ishisaka R, Okamoto H, Yamaguchi T (2016). "". J. Phys. Soc. Jpn.. **85**: 074703.
5. ^a ^b ^cVerdi C, Ranalli L, Franchini C, Kresse G (2023). ""Phys. Rev. Mater.. **7**: L030801.""
6. ^a ^b ^c ^d ^eYang F, Chen LQ (2024). "arXiv:2412.04308". arXiv. arXiv:2412.04308.
7. ^a ^bWu H, He R, Lu Y, Zhong Z (2022). "Phys. Rev. B." **106**: 224102.
8. ^Singh DJ (1996). "Title not provided". Phys. Rev. B. **53**: 176.
9. ^a ^b ^c ^d ^e ^f ^g ^h ^i ^j ^k ^lLi X, Qiu T, Zhang J, Baldini E, Lu J, Rappe AM, Nelson KA (2019). "Science". Science. **364**: 1079.
10. ^a ^b ^c ^d ^e ^f ^g ^h ^i ^j ^k ^l ^m ^n ^o ^pCheng B, Kramer PL, Shen Z-X, Hoffmann MC (2023). "Phys. Rev. Lett.". **130**: 126902.
11. ^Andrews S (1985). "Title not provided". J. Phys. C: Solid State Phys.. **18**: 1357.
12. ^Toulouse J, DiAntonio P, Vugmeister B, Wang X, Knauss L (1992). "Phys. Rev. Lett.". **68**: 232.
13. ^Aktas O, Crossley S, Carpenter MA, Salje EK (2014). "". Phys. Rev. B. **90**: 165309.
14. ^Rischau CW, Lin X, Grams CP, Finck D, Harms S, Engelmayer J, Lorenz T, Gallais Y, Fauque B, Hemberger J, et al. (2017). "". Nat. Phys.. **13**: 643.
15. ^Takesada M, Itoh M, Yagi T (2006). "". Phys. Rev. Lett.. **96**: 227602.
16. ^De La Torre A, Kennes DM, Claassen M, Gerber S, McIver JW, Sentef MA (2021). "Rev. Mod. Phys.". **93**: 041002.
17. ^Fechner M, F{"o}rst M, Orenstein G, Krapivin V, Disa A, Buzzi M, von Hoegen A, de la Pena G, Nguyen Q, Mankowsky R, et al. (2024). "". Nat. Mater.. **23**: 363.
18. ^Basini M, Pancaldi M, Wehinger B, Udina M, Unikandanunni V, Tadano T, Hoffmann M, Balatsky A, Bonetti S (2024). "Title not provided". Nature. pp. 1–6.
19. ^Nova T, Disa A, Fechner M, Cavalleri A (2019). "Science". Science. **364**: 1075.
20. ^Prosandeev S, Grollier J, Talbayev D, Dkhil B, Bellaiche L (2021). "Phys. Rev. Lett.". **126**: 027602.
21. ^Prosandeev S, Prokhorenko S, Nahas Y, Yang Y, Xu C, Grollier J, Talbayev D, Dkhil B, Bellaiche L (2022). "Phys. Rev. B". **105**: L100101.
22. ^a ^b ^cYamada Y, Shirane G (1969). "". J. Phys. Soc. Jpn.. **26**: 396.

23. ^ a b c *Fleury P, Worlock J (1968). ""Phys. Rev."". **174**: 613.*
24. ^ a b c *Sirenko A, Bernhard C, Golnik A, Clark AM, Hao J, Si W, Xi X (2000). "Nature". Nature. **404**: 373.*
25. ^ a b c *Shirane G, Nathans R, Minkiewicz V (1967). "". Phys. Rev.. **157**: 396.*
26. ^ a b c d e f g h i j k *Li X, Peng P, Dammak H, Geneste G, Akbarzadeh A, Prosandeev S, Bellaiche L, Talb ayev D (2023). "Phys. Rev. B." **107**: 064306.*
27. ^ *Zhuang Z, Chakraborty A, Chandra P, Coleman P, Volkov PA (2023). "". Phys. Rev. B. **107**: 224307.*
28. ^ *Shin D, Latini S, Schäfer C, Sato SA, Baldini E, De Giovannini U, Hübener H, Rubio A (2022). "". Phys. R ev. Lett.. **129**: 167401.*
29. ^ *Hafez HA, Kovalev S, Deinert J-C, Mics Z, Green B, Awari N, Chen M, Germanskiy S, Lehnert U, Teichert J, et al. (2018). "Nature". Nature. **561**: 507.*
30. ^ a b c d *Matsunaga R, Hamada YI, Makise K, Uzawa Y, Terai H, Wang Z, Shimano R (2013). "". Phys. Rev. Lett.. **111**: 057002.*
31. ^ a b c d *Matsunaga R, Tsuji N, Fujita H, Sugioka A, Makise K, Uzawa Y, Terai H, Wang Z, Aoki H, Shiman o R (2014). "Science". Science. **345**: 1145.*
32. ^ a b c d *Shimano R, Tsuji N (2020). "Annu. Rev. Condens. Matter Phys.". Annu. Rev. Condens. Matter Phy s.. **11**: 103.*
33. ^ a b *Yang F, Wu M (2018). "Phys. Rev. B". **98**: 094507.*
34. ^ a b *Cui T, Yang X, Vaswani C, Wang J, Fernandes RM, Orth PP (2019). "". Phys. Rev. B. **100**: 054504.*
35. ^ *Yang F, Wu M (2019). "Phys. Rev. B". **100**: 104513.*
36. ^ *Yang F, Wu M (2023). "". Ann. Phys.. **453**: 169312.*
37. ^ *Pekker D, Varma C (2015). "Annu. Rev. Condens. Matter Phys.". **6**: 269.*
38. ^ a b *Sivasubramanian S, Widom A, Srivastava Y (2004). "". Ferroelectrics. **300**: 43.*
39. ^ *Cochran W (1981). "". Ferroelectrics. **35**: 3.*
40. ^ *Cochran W (1961). "Title not provided". Adv. Phys.. **10**: 401.*
41. ^ *Cowley R (1965). "Title not provided". Phil. Mag.. **11**: 673.*
42. ^ *Cochran W (1969). "Title not provided". Adv. Phys.. **18**: 157.*
43. ^ *Cochran W (1960). "Title not provided". Adv. Phys.. **9**: 387.*
44. ^ *Yelon W, Cochran W, Shirane G, Linz A (1971). "Ferroelectrics". Ferroelectrics. **2**: 261.*
45. ^ *Peskin ME. An introduction to quantum field theory. CRC press; 2018.*
46. ^ *Chen LQ (2002). "". Annu. Rev. Mater. Res.. **32**: 113.*

47. ^ *Yang F, Wang L, Wu MW (2015). "". Phys. Rev. B. 92: 155414.*

48. ^ *Yang F, Wu MW (2016). "Phys. Rev. B". 93: 235433.*

49. ^ *Der Horst CA, Magnien S, Kapphan S (1996). Ferroelectrics. 185:265.*

50. ^ *Höchli U, Boatner L (1979). Phys Rev B. 20:266.*

51. ^ *Höchli U, Weibel H, Boatner L (1977). Phys Rev Lett. 39:1158.*

52. ^ *von Hoegen A, Mankowsky R, Fechner M, Först M, Cavalleri A (2018). Nature. 555:79.*

53. ^ *Grishunin KA, Ilyin NA, Sherstyuk NE, Mishina ED, Kimel A, Mukhortov VM, Ovchinnikov AV, Chefonov OV, Agranat MB (2017). Sci Rep. 7:687.*

54. ^ *Miyamoto T, Hata D, Morimoto T, Yamakawa H, Kida N, Terashige T, Iwano K, Kishida H, Horiuchi S, Okamoto H (2018). Sci Rep. 8:15014.*

Supplementary data: available at https://doi.org/10.32388/8Y19C2

Declarations

Funding: No specific funding was received for this work.

Potential competing interests: No potential competing interests to declare.